Quantization Error Analysis in Range Sensing by Active Triangulation

X. Y. Jiang, H. Bunke

IAM-93-002

May 1993

Quantization Error Analysis in Range Sensing by Active Triangulation

X. Y. Jiang, H. Bunke
Institut für Informatik und angewandte Mathematik
Universität Bern, Länggassstrasse 51, 3012 Bern, Switzerland

Abstract

Three-dimensional (3-D) methods in computer vision have been gaining increasing importance. Among the various range acquisition techniques, active triangulation is certainly the most common approach. In practice, the relationship between the geometry of an active triangulation system and the accuracy in obtaining three-dimensional position information is of great importance. In this paper we consider the error in position estimation due to the finite resolution of the imaging device. A point's measured position in the image plane maps to a small area in 3-D space. With the assumption that the point's true position is uniformly distributed inside this area, closed-form expressions for the probability distribution of error and the average error along each coordinate direction (horizontal, vertical, and range) are derived. Following this, the errors in the three coordinate directions are compared to each other. The probability that the error along one coordinate direction dominates that along another coordinate direction is inferred. The results presented in this paper have potential applications to range sensor configuration and error modeling in vision tasks using range data acquired by active triangulation.

CR Categories and Subject Descriptors: I.2.9 [Robotics]: Sensors.
Additional Key Words: Computer vision, range data acquisition, quantization error, position error analysis.

1 Introduction

Recently, three-dimensional (3-D) vision techniques based on range data have been receiving much attention in computer vision and robotics. Particularly, in such areas as industrial and navigational robotics where a robot must be capable of understanding its 3-D environment, range information plays a vital role. The need for 3-D vision techniques based on range data has led to the development of many range imaging techniques [2, 6, 7, 11]. Among them, active triangulation is certainly the most common approach.

A simple geometry for an active triangulation system is shown in Fig. 1. A projection device sends out a plane of light. The intersection of the light plane with the objects in the scene generates a stripe of light which is sensed by the camera. For each point P of the sensed stripe in the image plane, the actual 3-D position S can be determined by triangulation, i.e., by computing the intersection of the light plane and the straight line passing through P and the lens' center O. A single light plane gives range data on one stripe. Complete ranging of the scene requires a series of different light planes. In practice, this is achieved by displacing the projection device [15] or, equivalently, displacing the scene [5]. Another way is to project multiple light planes at one time. In this case the inherent ambiguities in identifying the different light planes are resolved by using binary coded or color coded projection patterns [1, 4, 12, 13, 14, 16].

The accuracy in 3-D position estimation is influenced by a number of factors like the accuracy of the system parameters, and the camera model. Another cause for range estimation errors is the finite resolution nature of the imaging device. As a matter of fact, the projection of the 3-D point S in the image plane, P, can only be determined with an uncertainty of $\pm\frac{1}{2}$ pixel for *any* pixel size. Consequently, the determined 3-D position of S is also subject to some uncertainty. The range estimation accuracy can be improved by decreasing the sampling interval, but this is usually constrained by the limitations in device technology and bandwidth.

Quantization errors due to the finite resolution of the imaging system have been analysed for some passive range sensing systems, for example, lateral stereo [3] and axial motion stereo [10]. In this paper we give such an error analysis for range sensing by active triangulation. We will derive closed-form expressions for the probability distribution of error and the average error along each coordinate direction (x, y, and range z). Following this, the errors in the three coordinate directions are compared to each other. The probability that the error along one coordinate direction dominates that along another coordinate direction is derived. In our analysis it will be assumed that the only cause of error is the image plane quantization in terms of a system of image coordinates. A pinhole camera model is used, thus ignoring camera lens distortion and other optical nonlinearities. Despite these simplifications, the results presented in this paper are still useful as they are upper bound performance estimates for any active triangulation system that processes sampled image data.

2 Active triangulation

Illustrated in Fig. 1 is the camera-centered active triangulation geometry. The camera is aligned along the z-axis with the lens' center located at the origin of the world coordinate system O. At a baseline distance Δ to the left of the camera (along the negative x-axis) is the projection device. The x-axis is defined to align with the scan line of the image plane. The y-axis is determined by the right-hand rule, thus pointing into the page. The quantity f denotes the focal length, while d_x and d_y are the horizontal and vertical pixel spacings of the

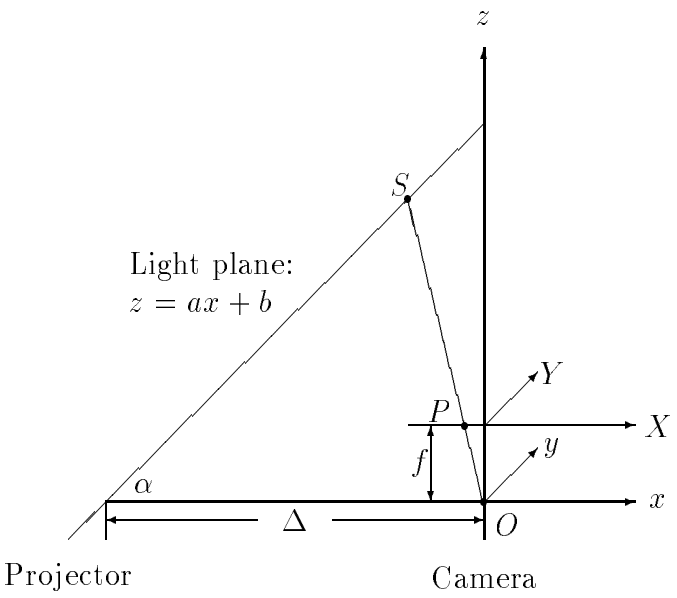

Figure 1: Camera-centered active triangulation geometry.

imaging space, respectively. In the image plane, we define an image pixel coordinate system (X, Y), where X and Y represent the column and row number of a pixel, respectively. The origin is located at the center of the image plane through which the optical axis passes. Let the projection of a 3-D point S onto the image plane, P, have the coordinates (U, V). Then in the world coordinate system, P will have the coordinates (u, v, f)[1] with

$$u = Ud_x, \quad v = Vd_y. \tag{1}$$

We assume that the light plane is perpendicular to the xz-plane. In other words, the normal of the light plane and the optical axis of the imaging device are coplanar. Under this assumption the light plane can be described by

$$z = ax + b, \quad a > 0, b > 0 \tag{2}$$

in the world coordinate system. This constraint imposes no serious restriction on the geometrical configuration of the camera and the projection device. As a matter of fact, it is even desired in order to come up with a simple calibration and an efficient realization of the triangulation [5, 16].

Given the active triangulation geometry, it is easy to derive the location of S in terms of the coordinates of P and the system parameters:

$$\begin{aligned} S(x, y, z) &= \left(\frac{bd_xU}{f - ad_xU}, \frac{bd_yV}{f - ad_xU}, \frac{bf}{f - ad_xU}\right) \\ &= \left(\frac{bu}{f - au}, \frac{bv}{f - au}, \frac{bf}{f - au}\right). \end{aligned} \tag{3}$$

It follows from (3) that an image pixel (U, V) uniquely determines the point in 3-D space which maps to that pixel.

[1] A pixel may be represented by integer indices (U, V) in the image pixel coordinate system, or equivalently by (u, v, f) in the world coordinate system. In the rest of this paper we will use either of the representations, whichever is more convenient.

3 Quantization error in 3-D point estimation

An implicit assumption made in (3) is that S projects exactly onto integer valued image coordinates. However, the exact location of the projection of S onto the image plane is usually not exactly at (U, V), but within a small area $(U \pm \frac{1}{2}, V \pm \frac{1}{2})$. This is due to the fact that a digital imaging device locates a projected point no more accurately than with the nearest integer valued coordinates. We can define the true location in the image plane as

$$U^* = U + n_x, \quad V^* = V + n_y \tag{4}$$

where n_x and n_y are real numbers between -$\frac{1}{2}$ and $\frac{1}{2}$. Then the true location of S is

$$\begin{aligned} S(x,y,z) &= \left(\frac{bd_xU^*}{f - ad_xU^*}, \frac{bd_yV^*}{f - ad_xU^*}, \frac{bf}{f - ad_xU^*}\right) \\ &= \left(\frac{b(u + d_xn_x)}{f - a(u + d_xn_x)}, \frac{b(v + d_yn_y)}{f - a(u + d_xn_x)}, \frac{bf}{f - a(u + d_xn_x)}\right). \end{aligned} \tag{5}$$

Clearly, the uncertainty in locating a 3-D point stems from the quantities n_x and n_y that are not physically obtainable in any finite resolution system.

3.1 Joint probability distribution of projection points

If we map the uncertainty area $(U \pm \frac{1}{2}, V \pm \frac{1}{2})$ back onto the light plane, we get a parallelogram PAR. That is, for any point in PAR, the imaging device will generate the same pixel (U, V). To quantify the amount of uncertainty in obtaining the location of the 3-D point S, we assume that the true position of S may lie anywhere *uniformly* within PAR. This model of uncertainty is reasonable since *a priori* information about the point S does not exist. This results in a probabilistic interpretation of n_x and n_y as continuous random variable N_x and N_y. Next, we derive the joint density function of N_x and N_y.

For some fixed n_x and n_y, the point P in the image plane has the coordinates $(u + d_xn_x, v + d_yn_y)$. Now let's consider a differential square A,

$$u + d_xn_x \leq X \leq u + d_xn_x + dx, \quad v + d_yn_y \leq Y \leq v + d_yn_y + dy. \tag{6}$$

If we map A back onto the light plane, we will get a differential parallelogram A'. Under the assumption that the true position of S lies anywhere uniformly within PAR, the probability that the random variables N_x and N_y take the value n_x and n_y, respectively, can be modeled as being proportional to the area of A'.

In order to compute the area of A', we project A' onto the xy-plane and get another parallelogram A''. The mapping from A to A'' corresponds to the tranformation

$$x' = \frac{bx}{f - ax}, \quad y' = \frac{by}{f - ax}. \tag{7}$$

Thus, from calculus (see for example [9]), the area of A'' can be computed[2],

$$A'' = |J(u + d_xn_x, v + d_yn_y)|dxdy \tag{8}$$

[2] As no confusion can occur, we use the same notation for parallelograms A, A', $\cdots$, and their area.

where $J(u+d_x n_x, v+d_y n_y)$ is the Jacobian of the transformation (7) at the point $(u+d_x n_x, v+d_y n_y)$. Actually computing the Jacobian yields

$$A'' = \frac{fb^2}{(f-a(u+d_x n_x))^3} dxdy. \tag{9}$$

Here we have used the fact that $f - ax > 0$ for all pixels (x, y, f) in the image plane (see Appendix A). This inequality will also be implicitly used many times in the rest of the paper.

From A'', the area of A' is easily computed by

$$A' = \frac{A''}{\cos\alpha} = \frac{fb^2}{\cos\alpha(f-a(u+d_x n_x))^3} dxdy \tag{10}$$

where α is the angle of the light plane relative to the x-axis. As the probability that the random variables N_x and N_y take the value n_x and n_y, respectively, is proportional to A', we get the joint density function of N_x and N_y by normalizing A',

$$f_{N_x,N_y}(n_x, n_y) = \frac{2ad_x C}{(f-a(u+d_x n_x))^3}, \quad -\tfrac{1}{2} \le n_x, n_y \le \tfrac{1}{2} \tag{11}$$

where

$$C = [\frac{1}{(f-a(u+\frac{d_x}{2}))^2} - \frac{1}{(f-a(u-\frac{d_x}{2}))^2}]^{-1} \tag{12}$$

is a constant.

3.2 Strategy of quantization error analysis

Given a pixel $P = (U, V)$, or expressed in the world coordinate system, $P = (u, v, f) = (Ud_x, Vd_y, f)$, we want to find out the uncertainty in the 3-D position reconstructed from (3). As will be shown later, each error E we want to analyse corresponds to a function $E = g(n_x, n_y)$ of the random variables n_x and n_y. Consequently, the probability that E is smaller than some limit ϵ can be determined by integration of the joint density function over an appropriate region R, i.e.,

$$prob(E < \epsilon) = \iint_R f_{N_x,N_y}(n_x, n_y)\, dn_x dn_y \tag{13}$$

where R consists of those pairs of (n_x, n_y)-values that satisfy $g(n_x, n_y) < \epsilon$. The average error of E is computed by

$$\bar{E} = \int_{-\frac{1}{2}}^{\frac{1}{2}}\int_{-\frac{1}{2}}^{\frac{1}{2}} g(n_x, n_y) f(n_x, n_y)\, dn_x dn_y. \tag{14}$$

For the case that the function g is a linear combination of its variables, i.e.,

$$g(x_1, x_2, \cdots, x_n) = |\alpha_1 x_1 + \alpha_2 x_2 + \cdots + \alpha_n x_n| \tag{15}$$

($n = 2$ in our case), general solutions are known for the integration problems stated above [8]. Concretely, the probability of E being smaller than ϵ is

$$prob(E < \epsilon) = 1 - \frac{2}{n!\tilde{\alpha}} \sum_{\sigma_1=\pm 1} \cdots \sum_{\sigma_n=\pm 1} \tilde{\sigma}(S-\epsilon)^n \cdot \theta(S-\epsilon) \tag{16}$$

where

$$\tilde{\alpha} = \prod_{i=1}^{n} \alpha_i, \quad \tilde{\sigma} = \prod_{i=1}^{n} \sigma_i, \quad S = \frac{1}{2} \sum_{i=1}^{n} \sigma_i \alpha_i \tag{17}$$

and θ is the Heaviside step function

$$\theta(t) = \begin{cases} 0 & \text{if } t \leq 0 \\ 1 & \text{if } t > 0 \end{cases} \tag{18}$$

Furthermore, the average error of E is computed by

$$\bar{E} = \frac{2}{(n+1)!\tilde{\alpha}} \sum_{\sigma_1=\pm 1} \cdots \sum_{\sigma_n=\pm 1} \tilde{\sigma} S^{n+1} \theta(S). \tag{19}$$

In our analysis we will use these general solutions in one particular case. For the other cases, either they are not applicable because g is not linear, or the integrals can be directly solved.

4 Analysis of position estimation errors

In this section we derive closed-form expressions for the probability distribution of error and the average error along x, y, and range z direction. Moreover, we compare the errors in the coordinate directions to each other. In each analysis case we follow the error analysis strategy described above and give results of simulations that were carried out to verify the theoretical results.

4.1 Error in range z

Let's define the relative error in ranging a point as

$$\epsilon_z = \left| \frac{z^* - z}{z} \right| \tag{20}$$

where z is the exact range of the point,

$$z = \frac{bf}{f - a(u + d_x n_x)} \tag{21}$$

and z^* is the quantized ranged point,

$$z^* = \frac{bf}{f - au}. \tag{22}$$

Substituting (21) and (22) into (20) gives

$$\epsilon_z = \frac{a d_x}{f - au} |n_x|. \tag{23}$$

As n_x takes value between -$\frac{1}{2}$ and $\frac{1}{2}$, i.e. $|n_x| \leq \frac{1}{2}$, $\epsilon_z \leq \frac{a d_x}{2(f - a u)}$ holds. Thus, the largest possible error in range z is

$$\tau_{z,max} = \frac{a d_x}{2(f - au)}. \tag{24}$$

Note that the quantity $\tau_{z,max}$ increases with u. Thus, among all image pixels, the largest $\tau_{z,max}$ is arrived at pixels in the rightmost column of the range image.

From (23), the probability that the relative error in range z, ϵ_z, is less than a specified tolerance $\tau_z (\leq \tau_{z,max})$ can be formulated as

$$\begin{aligned} P(\epsilon_z < \tau_z) &= P(\frac{ad_x}{f-au}|n_x| < \tau_z) \\ &= P(|n_x| < \frac{f-au}{ad_x}\tau_z). \end{aligned} \tag{25}$$

The task is now to integrate the joint density function of N_x and N_y (11) over the region in the $n_x n_y$-plane defined by the above equation. As the shape of this region is a simple rectangle, the integration is very easy. If we define $T = \frac{f-au}{ad_x}\tau_z$, then

$$\begin{aligned} P(\epsilon_z < \tau_z) &= \int_{-\frac{1}{2}}^{\frac{1}{2}} dn_y \int_{-T}^{T} f_{N_x,N_y}(n_x, n_y)\ dn_x \\ &= \begin{cases} C \cdot [\frac{1}{(f-a(u+Td_x))^2} - \frac{1}{(f-a(u-Td_x))^2}], & \tau_z < \tau_{z,max} \\ 1, & \tau_z \geq \tau_{z,max} \end{cases} \end{aligned} \tag{26}$$

It turns out that the probability expression (26) for error in range z can be simplified greatly. For this purpose we use the fact that $\pm Td_x$ is very small, so the value $(f-a(u \pm Td_x))^{-2}$ in (26) can be computed by the first order Taylor series approximation of the function $(f-ax)^{-2}$ at $x = u$,

$$\frac{1}{(f-a(u \pm Td_x))^2} \approx \frac{1}{(f-au)^2} \pm \frac{2a}{(f-au)^3} Td_x. \tag{27}$$

Similarly, the two terms in the constant C can be approximated by

$$\frac{1}{(f-a(u \pm \frac{d_x}{2}))^2} \approx \frac{1}{(f-au)^2} \pm \frac{2a}{(f-au)^3}\frac{d_x}{2}. \tag{28}$$

Substituting (27) and (28) into (26) and after some manipulations, we get the approximation expression

$$P(\epsilon_z < \tau_z) = \begin{cases} \frac{1}{\tau_{z,max}}\tau_z, & \tau_z < \tau_{z,max} \\ 1, & \tau_z \geq \tau_{z,max} \end{cases} \tag{29}$$

Recall that the only assumption made in the derivation of (26) is that the 3-D point S may lie anywhere uniformly within the parallelogram PAR in the light plane. Suppose we instead assume that the random variables N_x and N_y are independent and uniformly distributed between -$\frac{1}{2}$ and $\frac{1}{2}$. In this case their joint density function would be uniform,

$$f_{N_x,N_y}(n_x, n_y) = 1, \quad -\tfrac{1}{2} \leq n_x, n_y \leq \tfrac{1}{2}. \tag{30}$$

It can be shown that the resulting probability distribution of range error would be identical to (29). In the remaining discussions we will use (30) as an adequate approximation density function. This avoids lengthy computation and complicated formulas. In fact, simulation results show that this is an extremely good approximation.

Using this approximation density function we can compute the average error in z by

$$\begin{aligned} \bar{\epsilon_z} &= \int_{-\frac{1}{2}}^{\frac{1}{2}}\int_{-\frac{1}{2}}^{\frac{1}{2}} \frac{ad_x}{f-au}|n_x|\ dn_x dn_y \\ &= \tfrac{1}{2} \cdot \tau_{z,max} \end{aligned} \tag{31}$$

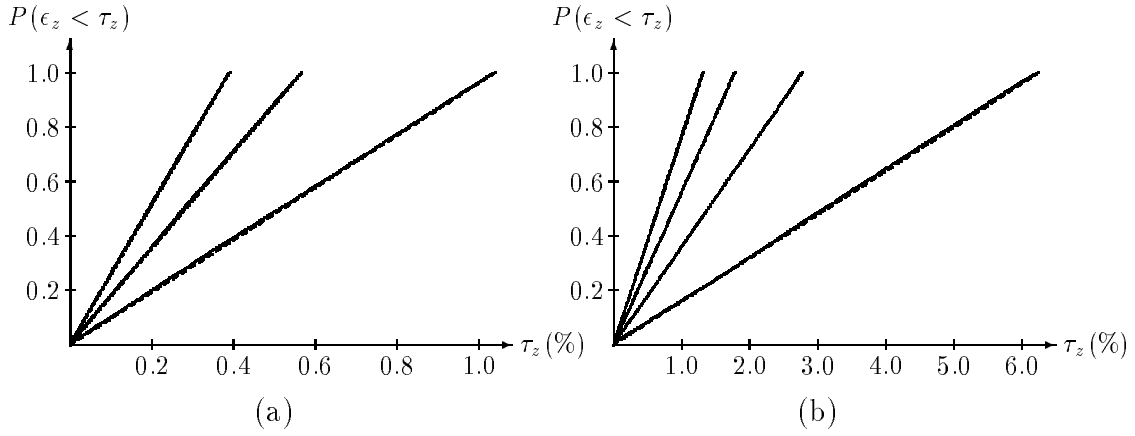

Figure 2: Cumulative distribution function of error in range. (a) From left to right: $(0, *)$, $(40, *)$, and $(80, *)$. (b) From left to right: $(90, *)$, $(100, *)$, $(110, *)$, and $(120, *)$.

We have performed simulations to verify the theoretical results derived above and in the subsequent sections. In all experiments described in this paper, the camera is a 512 by 512 pixel resolution imaging surface of dimension 50 mm by 38 mm (d_x= 0.098 mm, d_y= 0.074 mm). The focal length of the camera is 25 mm. The baseline distance is 500 mm. The angle α of the light plane relative to the x-axis is 63.4^o ($a = 2$, $b = 1000$ mm).

For the purpose of verification we consider a number of pixels $(U, *)$. (As the Y-coordinate is not involved in the error quantity investigated in this section, we take an arbitrary value for each pixel.) For each pixel $(U, *)$ under consideration, we randomly generate a large number (100000) of 3-D points located in the light plane which would project to the current pixel, and compute the error according to (20). Fig. 2(a) is a plot of the cumulative distribution functions for three pixels: $(0, *)$, $(40, *)$, and $(80, *)$. Fig. 2(b) shows the same function for four other pixels: $(90, *), (100, *), (110, *)$, and $(120, *)$. On the horizontal axis is the tolerance τ_z while the vertical axis denotes the probability $P(\epsilon_z < \tau_z)$ that the relative error in range ϵ_z does not exceed the tolerance. For each plotting, the theoretical function (29) is also shown (the dashed lines). Notice that the theoretical results express the experimental findings so closely that some of the dashed lines are scarcely visible. It turned out that the average error (31) is also very close to the experimental values. This is not surprising, due to the closeness of the theoretical and experimental error distribution.

4.2 Error in the horizontal direction x

In a way similar to Section 4.1 the probability distribution for position errors in the horizontal direction is now derived. We define the error in x direction as a function of range,

$$\epsilon_x = |\frac{x^* - x}{z}| \tag{32}$$

where

$$x = \frac{b(u + d_x n_x)}{f - a(u + d_x n_x)}, \quad x^* = \frac{bu}{f - au} \tag{33}$$

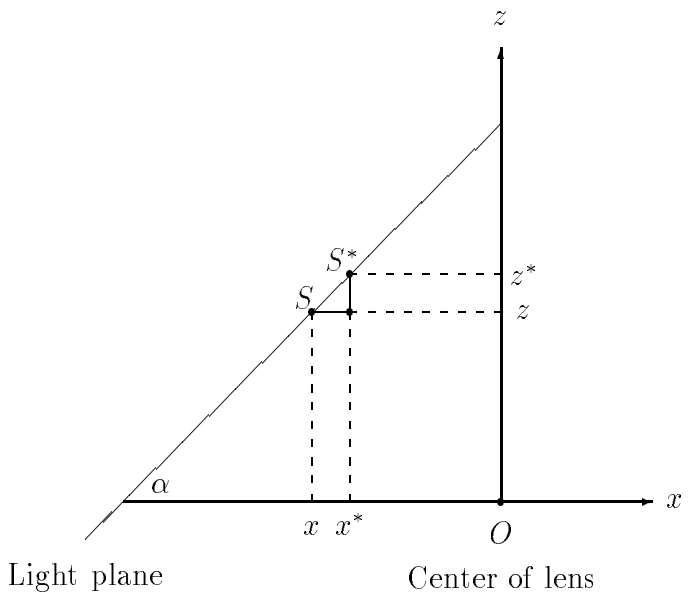

Figure 3: Relation between the errors in z and x direction.

are the true and measured horizontal position of an imaged point, respectively, and z is the exact range of the point. Substituting (33) and (21) into (32) yields

$$\epsilon_x = \frac{d_x}{f - au}|n_x| = \frac{1}{a}\epsilon_z. \tag{34}$$

This simple relation between the errors in z and x direction has a trivial geometrical interpretation, see Fig. 3. The point S^* is the estimated 3-D position of a point S based on the measured point in the image plane. Thus, we have

$$\frac{\epsilon_z}{\epsilon_x} = \frac{|z^* - z|}{|x^* - x|} = \tan\alpha. \tag{35}$$

As α is the angle of the light plane relative to the x-axis, $\tan\alpha = a$ holds. This gives (34) again, but in a geometrical way.

From (34), it is easy to see that the largest possible error in x is

$$\tau_{x,max} = \frac{d_x}{2(f - au)} = \frac{1}{a}\tau_{z,max}. \tag{36}$$

Similar to $\tau_{z,max}$, the quantity $\tau_{x,max}$ increases with u. Among all pixels, the largest $\tau_{x,max}$ is arrived at pixels in the rightmost column of the range image.

Using the uniform joint density function (30), the probability that the error in x, ϵ_x, is less than a specified tolerance $\tau_x (\leq \tau_{x,max})$ is given by

$$\begin{aligned} P(\epsilon_x < \tau_x) &= P(\frac{d_x}{f - au}|n_x| < \tau_x) \\ &= P(|n_x| < \frac{f - au}{d_x}\tau_x) \\ &= \begin{cases} \frac{1}{\tau_{x,max}}\tau_x, & \tau_x < \tau_{x,max} \\ 1, & \tau_x \geq \tau_{x,max} \end{cases} \end{aligned} \tag{37}$$

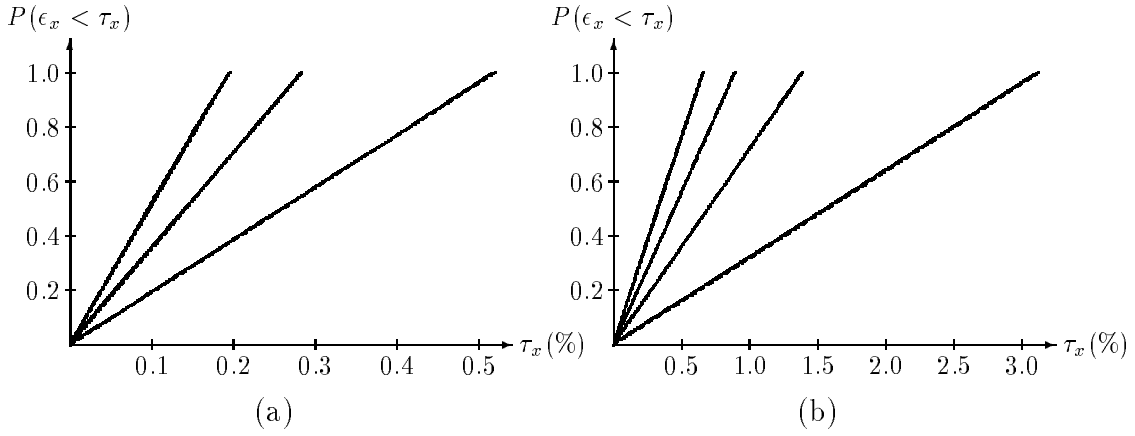

Figure 4: Cumulative distribution function of error in x. (a) From left to right: $(0, *)$, $(40, *)$, and $(80, *)$. (b) From left to right: $(90, *)$, $(100, *)$, $(110, *)$, and $(120, *)$.

The average error in x is computed by

$$\begin{aligned} \bar{\epsilon_x} &= \int_{-\frac{1}{2}}^{\frac{1}{2}} \int_{-\frac{1}{2}}^{\frac{1}{2}} \frac{d_x}{f - au} |n_x| \, dn_x dn_y \\ &= \tfrac{1}{2} \cdot \tau_{x,max} \end{aligned} \tag{38}$$

A simulation experiment was performed to verify (37). The experimental setup was identical to the one described in the last section. The same procedure was used to randomly generate 3-D points. In this experiment, however, we computed the error using (32). Fig. 4(a) is a representation of the cumulative distribution functions for three pixels of the range image: $(0, *)$, $(40, *)$, and $(80, *)$. Again, the Y-coordinate was not of interest and set to an arbitrary value. Fig. 4(b) shows the same function for four other pixels: $(90, *), (100, *), (110, *)$, and $(120, *)$. In each plotting, the theoretical function (37) is also drawn (the dashed lines).

4.3 Error in the vertical direction y

The probability distribution for position error in the vertical direction is now derived. We define the error in y direction as a function of range,

$$\epsilon_y = |\frac{y^* - y}{z}| \tag{39}$$

where

$$y = \frac{b(v + d_y n_y)}{f - a(u + d_x n_x)}, \quad y^* = \frac{bv}{f - au} \tag{40}$$

are the true and measured vertical position of an imaged point, respectively, and z is the exact range of the point. Let $R = \frac{d_x}{d_y}$ be the ratio of the sampling intervals in x and y direction. Substituting (40) and (21) into (39) yields

$$\epsilon_y = \frac{d_y}{f} |n_y + \frac{aRv}{f - au} n_x|. \tag{41}$$

Now we consider the largest possible error in y. Using the triangle inequality, we get

$$\begin{aligned} \epsilon_y &\leq \frac{d_y}{f}(|n_y| + \frac{aR|v|}{f-au}|n_x|) \\ &\leq \frac{d_y}{2f}(1 + \frac{aR|v|}{f-au}). \end{aligned} \tag{42}$$

It is easy to see that this upper bound can always be reached, say at $n_x = \frac{\mathrm{sgn}(v)}{2}, n_y = \frac{1}{2}$, where sgn is the sign function

$$\mathrm{sgn}(x) = \begin{cases} 1 & v \geq 0 \\ -1 & v < 0 \end{cases} \tag{43}$$

Thus, we have

$$\tau_{y,max} = \frac{d_y}{2f}(1 + \frac{aR|v|}{f-au}). \tag{44}$$

The quantity $\tau_{y,max}$ increases with u and $|v|$. Thus, among all pixels, the largest $\tau_{y,max}$ is arrived at the right lower and right upper corner of the range image.

From (41), the probability that the error in y, ϵ_y, is less than a specified tolerance $\tau_y (\leq \tau_{y,max})$ can be formulated as

$$\begin{aligned} P(\epsilon_y < \tau_y) &= P(\frac{d_y}{f}|n_y + \frac{aRv}{f-au}n_x| < \tau_y) \\ &= P(-\frac{aRv}{f-au}n_x - \frac{f}{d_y}\tau_y < n_y < -\frac{aRv}{f-au}n_x + \frac{f}{d_y}\tau_y). \end{aligned} \tag{45}$$

A direct integration over the region defined above is much more complicated than that for the derivation of error distributions for z and x. In fact, (45) reveals a region bounded by two parallel lines in the $n_x n_y$-plane. This region intersects the unit square $-\frac{1}{2} \leq n_x, n_y \leq \frac{1}{2}$ in many different ways. In this case the general integration formulas derived in [8] provide a much simpler solution. Let

$$A = \frac{aRv}{f-au}, \quad B = \frac{f}{d_y}\tau_y. \tag{46}$$

By using (16) we get

$$P(\epsilon_y < \tau_y) = \begin{cases} 2BD, & 0 < \tau_y < \frac{d_y}{2f}||A| - 1| \\ 1 - \frac{(1+|A|-2B)^2}{4|A|}, & \frac{d_y}{2f}||A| - 1| \leq \tau_y < \tau_{y,max} \\ 1, & \tau_y \geq \tau_{y,max} \end{cases} \tag{47}$$

where

$$D = \begin{cases} 1, & |A| \leq 1 \\ \frac{1}{|A|}, & |A| > 1 \end{cases} \tag{48}$$

Note that the probability above is only dependent on the absolute value of v. Thus, two pixels (U, V) and $(U, -V)$ have the same probability $P(\epsilon_y < \tau_y)$. The average error in y can be computed by (19),

$$\bar{\epsilon_y} = \begin{cases} \frac{d_y}{24f|A|}|(A+1)^3 - (A-1)^3| & |A| > 1 \\ \frac{d_y}{24fA}[(A+1)^3 + (A-1)^3] & |A| \leq 1 \end{cases} \tag{49}$$

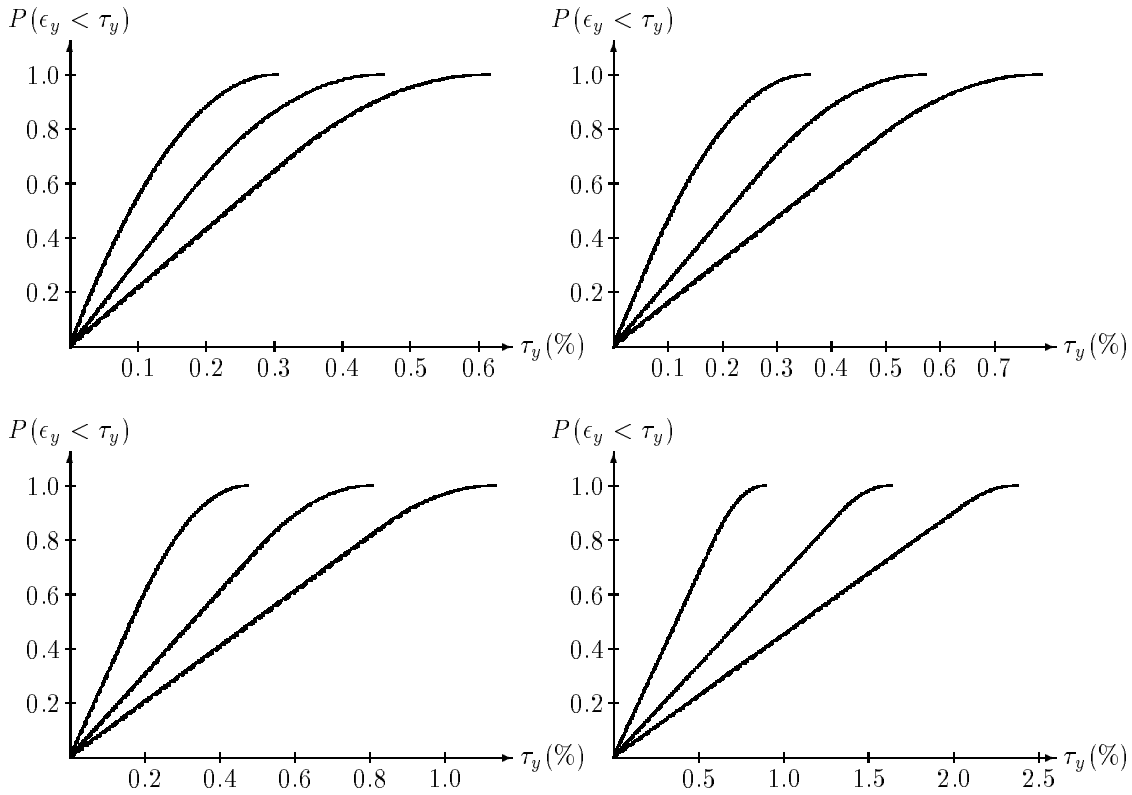

Figure 5: Cumulative distribution functions of error in y. Top left: $(90, *)$. Top right: $(100, *)$. Bottom left: $(110, *)$. Bottom right: $(120, *)$. In each diagram the three curves from left to right correspond to $V = 40, 80, 120$.

The correctness of (47) was verified by a simulation experiment using the same experimental setup and random 3-D point generation procedure as described earlier. In this experiment, we computed the error (39) for each generated 3-D point. In contrast to the error analysis for the horizontal and range direction, the error in vertical direction is also dependent on the Y-coordinate V of a pixel (U, V) in the range image. Fig. 5 plots the cumulative distribution functions for twelve pixels (U, V) where U takes the values 90, 100, 110, and 120, and V the values 40, 80, and 120. In each plotting, the theoretical function (47) is also drawn (the dashed lines). Note the closeness of the experimental and theoretical results. Also note that the error increases as U and V become larger.

4.4 Comparison between the errors in z and x

Until now we have derived probability distributions for position errors in each coordinate direction. What follows is to quantitatively compare the three errors. We begin with the simplest case, namely the comparison between the errors in z and x.

As shown in section 4.2, the errors in z and x satisfy

$$\epsilon_x = \frac{1}{a}\epsilon_z \tag{50}$$

where a is the slope of the light plane. If the angle of the light plane relative to the x-axis satisfies the inequality $\alpha < \frac{\pi}{4}$ $(a < 1)$, then the error in x is larger than that in z. Otherwise,

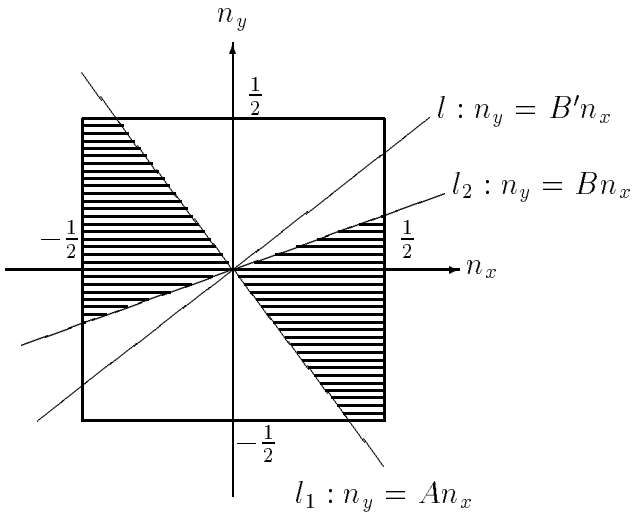

Figure 6: The $n_x n_y$-space.

the error in z is larger than that in x.

4.5 Comparison between the errors in z and y

As there doesn't exist such a simple relation like (50) between z and y, the analysis in this section is much more involved. We start by dividing (41) by (23),

$$\frac{\epsilon_y}{\epsilon_z} = \frac{f - au}{afR}|\frac{n_y}{n_x} + \frac{aRv}{f - au}|. \tag{51}$$

By defining

$$A = -\frac{aR(f + v)}{f - au}, \quad B = \frac{aR(f - v)}{f - au}, \tag{52}$$

the probability that the error in z is larger than that in y is given by

$$\begin{aligned} P(\epsilon_y < \epsilon_z) &= P(\frac{\epsilon_y}{\epsilon_z} < 1) \\ &= P(\frac{f - au}{afR}|\frac{n_y}{n_x} + \frac{aRv}{f - au}| < 1) \\ &= P(A < \frac{n_y}{n_x} < B). \end{aligned} \tag{53}$$

Here the general solution in [8] is not applicable as the function $g(n_x, n_y)$ is not a linear combination of n_x and n_y. Fortunately, the shape of the region defined by the above equation is quite simple, see the shaded region in Fig. 6. It is just that part of the unit square $-\frac{1}{2} \leq n_x, n_y \leq \frac{1}{2}$ that is generated by counterclockwise rotating l_1 towards l_2. This region intersects the unit square consisting of realizable values of n_x and n_y in many different ways. So we must consider all possible intersection cases. The actual analysis of all these cases is rather tedious.

	V=0	V=20	V=40	V=60	V=80	V=100	V=120
U=-120	0.6319	0.6304	0.6266	0.6198	0.6099	0.5968	0.5829
	0.6319	0.6284	0.6250	0.6212	0.6094	0.5982	0.5842
U=-80	0.6913	0.6902	0.6868	0.6811	0.6728	0.6614	0.6464
	0.6906	0.6916	0.6860	0.6800	0.6717	0.6615	0.6472
U=-40	0.7506	0.7497	0.7471	0.7425	0.7357	0.7265	0.7144
	0.7514	0.7480	0.7461	0.7427	0.7359	0.7264	0.7136
U=0	0.8100	0.8093	0.8073	0.8038	0.7986	0.7916	0.7824
	0.8102	0.8099	0.8092	0.8003	0.7970	0.7922	0.7844
U=40	0.8694	0.8689	0.8675	0.8651	0.8616	0.8567	0.8504
	0.8696	0.8697	0.8679	0.8656	0.8628	0.8585	0.8518
U=80	0.9287	0.9285	0.9277	0.9264	0.9245	0.9219	0.9184
	0.9262	0.9289	0.9265	0.9266	0.9248	0.9224	0.9185
U=120	0.9881	0.9881	0.9880	0.9877	0.9874	0.9870	0.9864
	0.9881	0.9879	0.9880	0.9876	0.9873	0.9867	0.9861

Table 1: Probability that range error ϵ_z exceeds vertical error ϵ_y. In each table position, the upper entry is the theoretical and the lower entry the experimentally determined value.

We give only the final result,

$$P(\epsilon_y < \epsilon_z) = \begin{cases} \frac{B-A}{4AB}, & |A| \geq 1, |B| \geq 1 \\ \frac{1+2A+AB}{4A}, & A \leq -1, -1 \leq B \leq 1 \\ \frac{-A+B+4AB}{4AB}, & A \leq -1, B \geq 1 \\ \frac{B-A}{4}, & -1 \leq A \leq 1, -1 \leq B \leq 1 \\ \frac{-1+2B-AB}{4B}, & -1 \leq A \leq 1, B \geq 1 \end{cases} \tag{54}$$

It is easy to prove that the above expression is only dependent on the absolute value of v. Thus, two pixels (U, V) and $(U, -V)$ have the same probability $P(\epsilon_y < \epsilon_z)$.

The above result was checked by performing a simulation experiment using the same triangulation setup and 3-D point generation procedure as described earlier. For each generated 3-D point, the errors in range and y due to the triangulation quantization were computed. The proportion of the points which have larger ϵ_z than ϵ_y was interpreted as the probability $P(\epsilon_y < \epsilon_z)$. In Table 1, the theoretical values (54) and the experimental values are listed for 49 pixels in the range image. Due to the symmetry in the Y-coordinate in (54), only pixels with positive Y-values are included in the table. Notice the closeness of the analytical and experimental results.

So far we have derived the expression for the probability that the range error ϵ_z exceeds the vertical error ϵ_y for some pixel (U, V) in the range image. Now we consider all pixels of the range image and figure out the region where the range error is more likely to be larger than the vertical error, i.e. $P(\epsilon_y < \epsilon_z) > 0.5$.

For this purpose, we make use of the fact that the approximated joint density function (30) is uniform. Thus, the probability $P(\epsilon_y < \epsilon_z)$ is just the area of the shaded region in Fig. 6.

This area is larger than 0.5 if and only if $B > B'$ holds where

$$B' = \frac{f - au}{aR(f + v)} \tag{55}$$

is the slope of the line l perpendicular to l_1. Substituting (52) and (55) into the inequality yields

$$\frac{aR(f - v)}{f - au} > \frac{f - au}{aR(f + v)}. \tag{56}$$

After some manipulations we get

$$(\frac{u - \frac{f}{a}}{Rf})^2 + (\frac{v}{f})^2 < 1. \tag{57}$$

Expressed in the image coordinates by using (1), (57) becomes

$$(\frac{U - \frac{f}{a d_x}}{\frac{Rf}{d_x}})^2 + (\frac{V}{\frac{f}{d_y}})^2 < 1 \tag{58}$$

which is an ellipse with the center $(\frac{f}{a d_x}, 0)$ and axis lengths $\frac{2Rf}{d_x}$ and $\frac{2f}{d_y}$. For all pixels within this ellipse, the range error ϵ_z is more likely to be larger than the vertical error ϵ_y.

As an illustration example, we assume a triangulation setup with $a = 1, d_x = d_y = d$ $(R = 1)$. Now the ellipse (58) becomes a circle

$$(U - \frac{f}{d})^2 + V^2 < (\frac{f}{d})^2 \tag{59}$$

with the center $(\frac{f}{d}, 0)$ and radius $\frac{f}{d}$. Thus, only for less than half of the pixels in the range image, the range error is more likely to be larger than the vertical error.

4.6 Comparison between the errors in x and y

This comparison proceeds as in the last section. We devide (41) by (34),

$$\frac{\epsilon_y}{\epsilon_x} = \frac{f - au}{fR} |\frac{n_y}{n_x} + \frac{aRv}{f - au}|. \tag{60}$$

By defining

$$A^* = -\frac{R(f + av)}{f - au}, \quad B^* = \frac{R(f - av)}{f - au}, \tag{61}$$

the probability that the error in x is larger than that in y is given by

$$\begin{aligned} P(\epsilon_y < \epsilon_x) &= P(\frac{\epsilon_y}{\epsilon_x} < 1) \\ &= P(\frac{f - au}{fR} |\frac{n_y}{n_x} + \frac{aRv}{f - au}| < 1) \\ &= P(A^* < \frac{n_y}{n_x} < B^*). \end{aligned} \tag{62}$$

	V=0	V=20	V=40	V=60	V=80	V=100	V=120
U=-120	0.3396	0.3396	0.3396	0.3396	0.3396	0.3380	0.3338
	0.3416	0.3384	0.3412	0.3377	0.3386	0.3387	0.3355
U=-80	0.4049	0.4049	0.4049	0.4027	0.3970	0.3885	0.3779
	0.4066	0.4044	0.4096	0.4043	0.3954	0.3897	0.3770
U=-40	0.5013	0.4980	0.4896	0.4775	0.4625	0.4453	0.4264
	0.5038	0.5015	0.4913	0.4781	0.4635	0.4446	0.4292
U=0	0.6200	0.6146	0.5973	0.5717	0.5439	0.5144	0.4836
	0.6201	0.6180	0.5978	0.5716	0.5461	0.5163	0.4829
U=40	0.7388	0.7350	0.7231	0.7008	0.6626	0.6124	0.5613
	0.7390	0.7348	0.7260	0.7016	0.6619	0.6122	0.5595
U=80	0.8575	0.8555	0.8490	0.8368	0.8160	0.7799	0.7106
	0.8572	0.8547	0.8490	0.8362	0.8161	0.7826	0.7117
U=120	0.9762	0.9759	0.9748	0.9728	0.9693	0.9633	0.9518
	0.9759	0.9761	0.9751	0.9727	0.9694	0.9637	0.9525

Table 2: Probability that horizontal error ϵ_x exceeds vertical error ϵ_y. In each table position, the upper entry is the theoretical and the bottom entry experimentally determined value.

In the same fashion as in the last section, we get the final result,

$$P(\epsilon_y < \epsilon_x) = \begin{cases} \frac{B^*-A^*}{4A^*B^*}, & |A^*| \geq 1, |B^*| \geq 1 \\ \frac{1+2A^*+A^*B^*}{4A^*}, & A^* \leq -1, -1 \leq B^* \leq 1 \\ \frac{-A^*+B^*+4A^*B^*}{4A^*B^*}, & A^* \leq -1, B^* \geq 1 \\ \frac{B^*-A^*}{4}, & -1 \leq A^* \leq 1, -1 \leq B^* \leq 1 \\ \frac{-1+2B^*-A^*B^*}{4B^*}, & -1 \leq A^* \leq 1, B^* \geq 1 \end{cases} \tag{63}$$

Note that the above expression is only dependent on the absolute value of v. Thus, two pixels (U, V) and $(U, -V)$ have the same probability $P(\epsilon_y < \epsilon_x)$.

Analogous to the last section, the probability expression above was tested by simulation. For 49 pixels in the range image, the results are shown in Table 2. Note again the closeness of the analytical and experimental results.

Now we try to find out the region in the range image where the horizontal error ϵ_x is more likely to be larger than the vertical error ϵ_y, i.e. $P(\epsilon_y < \epsilon_x) > 0.5$. The analysis is similar to the last section and we give only the final result. The region is an ellipse

$$\left(\frac{u - \frac{f}{a}}{\frac{Rf}{a}}\right)^2 + \left(\frac{v}{\frac{f}{a}}\right)^2 < 1 \tag{64}$$

or expressed in the image coordinates

$$\left(\frac{U - \frac{f}{a d_x}}{\frac{Rf}{a d_x}}\right)^2 + \left(\frac{V}{\frac{f}{a d_y}}\right)^2 < 1 \tag{65}$$

with the center $(\frac{f}{ad_x}, 0)$ and axis lengths $\frac{2Rf}{ad_x}$ and $\frac{2f}{ad_y}$. For all pixels within this ellipse, the horizontal error is more likely to be larger than the vertical error.

As an example, we assume a triangulation setup with $d_x = d_y = d$ $(R = 1)$. Now (65) becomes a circle

$$(U - \frac{f}{ad})^2 + V^2 < (\frac{f}{ad})^2 \tag{66}$$

with the center $(\frac{f}{ad}, 0)$ and radius $\frac{f}{ad}$. Thus, only for less than half of the pixels in the range image, the horizontal error is more likely to be larger than the vertical error.

5 Summary and discussion

In this paper we have quantified some fundamental limitations in the accuracy of obtaining 3-D positional information based on an active triangulation technique. In our analysis the camera model was an ideal pinhole camera, thus ignoring the camera lens distortion and other optical nonlinearities. Assuming the quantization error to be the single source of error, we have derived

- (29): the probability that the relative error in range is less than a specified tolerance,
- (31): the average error in z,
- (37): the probability that the horizontal positional error is less than a specified tolerance,
- (38): the average error in x,
- (47): the probability that the vertical positional error is less than a specified tolerance,
- (49): the average error in y,
- (50): the relation between the range error and the horizontal positional error,
- (54): the probability that the range error is larger than the vertical positional error,
- (58): describing the area in the range image where the range error is more likely to be larger than the vertical error,
- (63): the probability that the horizontal positional error is larger than the vertical error,
- (65): describing the area in the range image where the horizontal error is more likely to be larger than the vertical error.

These results represent the upper bounds of performance of any active triangulation based range acquisition system. We expect that the analysis presented here will have some impact on both range sensor configuration and error modeling in vision applications using range data acquired by active triangulation.

One possible application of the error analysis presented in this paper is the configuration of range data acquisition systems for industrial automation tasks, like robotics assembly or inspection and quality control. According to the terminology introduced in this paper, any range data acquisition system has the configuration parameters a, f, d_x, and d_y. If it is required, for example, that the error in x, y, or z doesn't exceed certain limits, then the equations derived in the previous sections can be used to find possible values of the configuration parameters such that the given requirements are met. Similarly, for a given configuration of the sensor system

and objects of approximately known size and shape, the equations can be used to derive possible locations and orientations for the objects being presented such that the measurement errors are minimized.

Appendix A

Here we show that, for all pixels (x, y, f) which are mapping of some point in the light plane onto the image plane, $f - ax > 0$ holds.

If $x \leq 0$, then the inequality is trivial. Let us assume $x > 0$. Referring to Fig. 1, the pixel $P = (x, y, f)$ is the mapping of some 3-D point in the light plane onto the image plane if and only if the line passing through P and the origin O has a larger slope than a, i.e.,

$$\frac{f}{x} > a. \tag{67}$$

Thus, we have $f - ax > 0$.

References

[1] M. D. Altschuler, et al., "Robot vision by encoded light beams", in T. Kanade (Ed.), Three-dimensional machine vision, 97–149, Kluwer Academic Publishers, 1987.

[2] P. J. Besl, "Active, optical range imaging sensors", Machine Vision and Applications, Vol. 1, 127–152, 1988.

[3] S. D. Blostein and T. S. Huang, "Error analysis in stereo determination of 3-D point positions", IEEE Trans. PAMI, Vol. 9, No. 6, 752–765, 1987.

[4] K. L. Boyer and A. C. Kak, "Color-encoded structured light for rapid active ranging", IEEE Trans. PAMI, Vol. 9, No. 1, 14–28, 1987.

[5] H. Hügli and G. Maître, "3D by structured light: Implementation and evaluation of a vision system for small parts", In A. Gruen and H. Kahmen (Eds.), Optical 3-D measurement techniques, 153–163, Wichmann, 1989.

[6] R. A. Jarvis, "A perspective on range finding techniques for computer vision", IEEE Trans. PAMI, Vol. 5, No. 2, 122-139, 1983.

[7] A. C. Kak, "Depth perception for robot vision", In S. Nof (Ed.), Handbook of Industrial Robots, Wiley, New York, 272–319, 1985.

[8] B. Kamgar-Parsi and B. Kamgar-Parsi, "Evaluation of quantization error in computer vision", IEEE Trans. PAMI, Vol. 11, No. 9, 929–940, 1989.

[9] S. Lang, "Calculus of several variables", Second Edition, Addison-Wesley Publishing Company, 1979.

[10] T. C. Nguyen and T. S. Huang, "Quantization errors in axial motion stereo on rectangular-tessellated image sensor", Proc. of 11th ICPR, Vol. I, 13–16, 1992.

[11] D. Nitzan, "Three-dimensional vision structure for robot applications", IEEE Trans. PAMI, Vol. 10, No. 3, 291–309, 1988.

[12] J. Potsdamer and M. Altschuler, "Surface measurement by space-encoded projected beam system", Computer Graphics and Image Processing, Vol. 18, 1–17, 1982.

[13] J. P. Rosenfeld, "A ranging system based on space coding for postal applications", Proc. of U.S. Postal Services Advanced Technology Conference, 43–57, 1988.

[14] K. Sato, H. Yamamoto and S. Inokuchi, "Tuned range finder for high precision 3D data", Proc. of 8th ICPR, Paris, 1168–1171, 1986.

[15] Y. Shirai and M. Suwa, "Recognition of polyhedrons with a range finder", Proc. of 2nd IJCAI, London, 80–87, 1971.

[16] T. G. Stahs and F. M. Wahl, "Fast and robust range data acquisition in a low-cost environment", Proc. of ISPRS-Conference, SPIE Vol. 1395, Zurich, 496–503, 1990.